18.12.2014

Summary of SEM Grid Test Measurements

Author(s): A. Reiter, M. Witthaus Version 0.4

History

24.06.2014	A. Reiter: Document creation
14.11.2014	A. Reiter: Add Ni data (14th of August) of HTP experiment Add estimates for minimum required particle numbers Add pictures of 8E7 raw data and noise structure
03.11.2014	M.Witthaus: Add Xe data (21st of September) of HTP experiment Add pictures of 8E6 raw data Add pictures and values of noise measurement
18.12.2014	A. Reiter: Add new plots in chapter 4 for 20 µs Shorten document (chapter 1 removed)

Abstract

This document summarises measurements that investigate the SEM grid response and performance of readout hardware. The measurements were performed in the HTP beam line with beams of 300 MeV/u and fast extraction from the SIS18 synchrotron.

Section 1 presents analytical formulae that provide estimates of the total charge ejected from a SEM grid for a given ion beam. These formulae have been verified against experimental data and are expected to predict SEM grid charges typically within a factor of 2. These estimates are applied to calculate the hardware response to typical HEBT beams and minimum required particle numbers for meaningful measurements are derived from a simple model.

Section 2 presents results of SEM grid measurements with Nickel and Xenon beams of 300 MeV/u kinetic energy after fast extraction from the SIS18 synchrotron (h=4). For the Nickel beam SEM grid profiles were simulated on the basis of the measured beam distribution, obtained from a Cromox screen, with a simple Monte Carlo code and compared to the experimental data with satisfactory agreement.

Section 3 presents noise levels of the new QFW hardware that were measured with a test setup in the laboratory.

Section 4 summarises observations and results.

TABLE OF CONTENTS

1 SEM Grid Signal Estimate

The SEM Grid response can be approximated on the basis of the secondary electron emission (SEE) yield of a single wire or foil and a simple geometric SEM Grid model. This model has been compared with experimental data and typically predicts the generated SEM charge within a factor of 2 which is sufficient for the purpose of defining the expected dynamic range of the readout hardware.

1.1 Secondary Electron Emission Yield

1.1.1 Theoretical yield - Sternglass theory

The theory of Sternglass has been published in reference [18]. It estimates the backward yield of secondary electron emission for low-energy ion impact.
The estimates presented in this document for high-energy particles - that penetrate the foil or wire material of a SEM Grid - are based on this model assuming identical yields for forward emission Y_F and backward emission Y_B, although typically $Y_F > Y_B$ holds at higher particle energies. Nevertheless, the assumption is justified on the basis of comparison of the total yields with numerous experimental data (see Appendix I).

1.1.2 Experimental yield - Rothard data

A useful rule of thumb is given in Ref. [1] for the total SEE yield Y_T for any target and any ion. It can be modified to read:

$$Y_T = 3 \cdot dE/dX\ [MeV/(mg/cm^2)] \cdot density\ [g/cm^3]$$

As stated by the authors, the estimate is thought to be correct within a factor of 2.

1.2 Integral SEM Grid Yield

To measure a beam profile, the total net charges of all SEM grid wires are registered individually during a given integration time, e.g. by charge integrators or I/U converters (IBT electronics) or charge-to-frequency converters (QFW). For each impacting ion, the net charge Q_{Net} per interaction is given by:

$$Q_{Net} = (q_{Ion}(in) + 2 \cdot Y - q_{Ion}(out))\ e,$$

where $q_{Ion}(in)$ and $q_{Ion}(out)$ are the charge states when the ion enters the foil and when it leaves the foil, respectively, e is the elementary charge and Y is the SEE yield. The values of $q_{Ion}(out)$ are calculated from the equilibrium charge state fits of Schiwietz (see references [11] and [12]).

A basic model estimates the total SEE yield:

- Calculation of the differential energy loss dE/dX by ATIMA [10] in units MeV/(g/cm^2) for a particle of atomic charge Z, mass number A, and charge Q.
- Calculation of the SEE yield Y_B according to the Sternglass model.
- The ejected electrons represent a positive charge on the wire, and together with the charges of the ion, the total net charge Q_{Net} per ion is given by
$$Q_{Net} = (q_{Ion}(in) + 2 \cdot Y_B - q_{Ion}(out)) e$$
- For a given number of ions N_{ion}, calculate the charge of a totally intercepting foil: $Q_{FOIL} = N_{ion} \cdot Q_{Net}$
- Correct for the geometric acceptance of the SEM grid, given by the ratio of wire diameter to wire separation in a simple approach:
$$acc = \text{wire diameter/wire separation}$$
- Calculate the total, integrated SEM grid charge Q_{SEM} :
$$\begin{aligned} Q_{SEM} &= acc \cdot Q_{FOIL} \\ &= acc \cdot N_{ion} \cdot Q_{Net} \\ &= acc \cdot N_{ion} \cdot (q_{Ion}(in) + 2 \cdot Y_B - q_{Ion}(out)) e \end{aligned}$$

Note that this is a very simplistic model, but for charge estimates within a factor of 2 the model is appropriate. Model predictions are compared to measured SEM grid charge values in Appendix II.

1.3 Model Predictions

The estimates of this section are calculated for pilot ion beams of 10^8 particles.

1.3.1 Integral SEM Grid Yields

Estimated total numbers of QFW counts have been calculated, assuming a sensitivity of 250 fC/count in most sensitive QFW range, for 10^8 ions in a Tungsten SEM Grid with coverage factor of 50%. Examples of SIS18 beams are compiled in Table 1 and of SIS100 beams in Table 2. For each ion the cases of minimum and maximum kinetic energy are considered. Light ions producing a total number of QFW counts below 100 are marked in red colour; Nickel and Xenon for which experimental data are available are marked in blue colour.

Table 1: SIS18 beams and total number of QFW counts for 1x10^8 primaries and 50% coverage

Ion	Z	A	q [e]	Kin. Energy [GeV/u]		Yield [e-/prim.]		SEM Grid Charge [nC]		SEM Grid Counts [250 fC/count]	
				E_{Min}	E_{Max}	E_{Min}	E_{Max}	E_{Min}	E_{Max}	E_{Min}	E_{Max}
proton	1	1	1	1,92	4,55	0,045	0,047	3,6E-04	3,8E-04	1,4E+00	1,5E+00
Ne	10	20	7	0,40	1,18	6,6	4,8	2,9E-02	1,4E-02	1,1E+02	5,7E+01
Ar	18	40	18	0,60	1,67	18,3	15,1	1,5E-01	1,2E-01	5,9E+02	4,9E+02
Ni	28	58	26	0,60	1,66	44,9	37,2	3,4E-01	2,8E-01	1,4E+03	1,1E+03
Kr	36	84	34	0,50	1,44	79,4	62,8	6,2E-01	4,9E-01	2,5E+03	1,9E+03
Xe	54	132	48	0,42	1,24	195,0	147,7	1,5E+00	1,1E+00	6,1E+03	4,5E+03
Au	79	197	65	0,36	1,08	450,3	334,3	3,5E+00	2,6E+00	1,4E+04	1,0E+04
U	92	238	28	0,05	0,20	1339,6	774,5	1,0E+01	5,7E+00	4,1E+04	2,3E+04
U	92	238	73	0,31	0,97	638,2	468,0	5,0E+00	3,6E+00	2,0E+04	1,4E+04

Table 2: SIS100 beams and total number of QFW counts for 1x10^8 primaries and 50% coverage

Ion	Z	A	q [e]	Kin. Energy [GeV/u]		Yield [e-/prim.]		SEM Grid Charge [nC]		SEM Grid Counts [250 fC/count]	
				E_{Min}	E_{Max}	E_{Min}	E_{Max}	E_{Min}	E_{Max}	E_{Min}	E_{Max}
proton	1	1	1	2,79	29,08	0,045	0,058	3,6E-04	4,7E-04	1,5E+00	1,9E+00
Ne	10	20	7	0,64	9,61	5,5	5,2	2,0E-02	1,7E-02	7,9E+01	7,0E+01
Ar	18	40	18	0,36	6,63	22,3	16,2	1,8E-01	1,3E-01	7,1E+02	5,2E+02
Ni	28	58	26	0,34	6,37	56,1	39,7	4,3E-01	3,0E-01	1,7E+03	1,2E+03
Kr	36	84	34	0,25	5,21	109,1	65,0	8,6E-01	5,0E-01	3,4E+03	2,0E+03
Xe	54	132	48	0,18	4,15	296,0	147,4	2,3E+00	1,1E+00	9,3E+03	4,5E+03
Au	79	197	65	0,11	2,99	779,1	322,0	6,2E+00	2,5E+00	2,5E+04	9,9E+03
U	92	238	28	0,09	2,72	1083,5	443,9	8,2E+00	3,0E+00	3,3E+04	1,2E+04
U	92	238	73	0,51	8,32	541,2	480,1	4,2E+00	3,7E+00	1,7E+04	1,5E+04

1.3.2 Estimate of Minimum Particle Number

We estimate the minimum particle number N_{Min} required for a "meaningful profile measurement" starting from a few simple assumptions:

- Coverage factor 10%, typical for SEM Grids at GSI
- Assume that 10 wires are covered by the beam spot
- Require 50 counts in the central wire, hence, the required grid integral is 250 QFW counts for a triangular profile shape

Using the estimates of Table 1, about 250 QFW counts (or 1250 counts for 50% coverage) are produced by 1x10^8 Ni ions. Scaling by the energy loss of a specific ion dE/dX which governs the SEE yield Y, the required ion numbers of Table 3 are calculated.

Table 3: Minimum particle number N_{Min} for ion species of Table 1 and 10% coverage factor

Ion	Z	A	Q	N_{Min}
proton	1	1	1	$1x10^{11}$
Ne	10	20	7	$1.2x10^{9}$
Ar	18	40	18	$2.3x10^{8}$
Ni	28	58	26	$1x10^{8}$
Kr	36	84	34	$5.4x10^{7}$
Xe	54	132	48	$2.2x10^{7}$
Au	79	197	65	$1x10^{7}$
U	92	238	28	$6.8x10^{6}$
U	92	238	73	$3.4x10^{6}$

Note:

- The estimate of 10^8 compared well with the experimental limit derived from the Nickel and Xenon measurements (see sections 2.1.2 and 2.2.2).
- If 10^8 minimum-ionising protons are to be measured with a SEM grid of 10% coverage, a total charge of 80 fC is ejected from all wires. Therefore, required charge resolution must be of the order of ~1 fC, about a factor 250 smaller than the QFW sensitivity.

Detour: Calculation of current emitted from a central wire by Uranium ions

- We assume that 10% of the beam interact in the wire
- The mean current I_{Mean} for a 50 ns pulse can easily be calculated:
  I_{Mean} = 0.5 nC / 50 ns ~ 0.01 A = 10 mA for 10^8 Uranium ions in the pulse.
- For a triangular pulse shape, the peak current I_{peak} is 0.02 A = 20 mA.
- A pulse of 10^{12} Uranium ions produces an instantaneous peak current I_{peak} of 200 A!

1.3.3 Differential SEM Grid Yields – Beam Profiles

Monte Carlo simulations for different ion species and a Gaussian beam of 0.75 cm standard deviation (beam spot size ~ 3 cm or 4σ) are presented in Figure 1 for a few selected ions of maximum SIS18 kinetic energy. Note the scaling factor of 1000 for the cases of Xenon and Uranium.
The beam spot size varies across the HEBT beam lines in the range of 1 to 6 cm. The QFW response is scaled to 10^8 primaries for a sensitivity of 250 fC/count. In this case, the coverage factor was increased to 50% which seems more realistic for the new HEBT SEM Grids.

The SEM Grid geometry was defined as:

- Material: Tungsten
- Geometry: 0.25 cm strips
  0.25 cm gap size (50% geometric coverage)

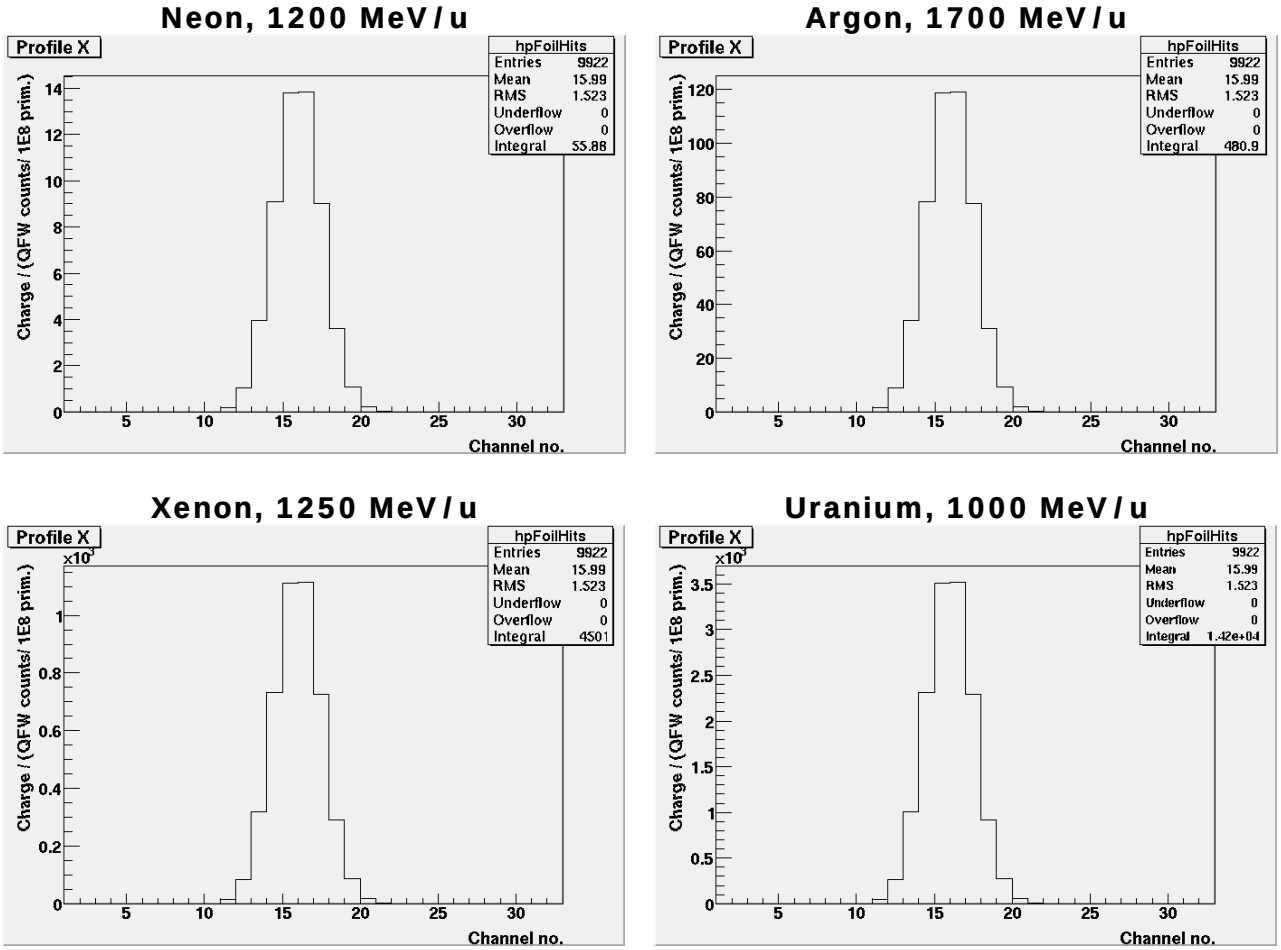

Figure 1: Simulated horizontal beam profiles for a DG090 profile grid. Note the different scales on the Y axis for Xenon and Uranium (x1000).

1.4 Comparison of IBT and QFW Sensitivity

In this section we try to compare the sensitivities of the existing IBT I/U converter electronics (used at HTP for normal accelerator operation) and of the new charge-to-frequency converter QFW.

1.4.1 IBT Electronics

The numbers presented here were taken from the manual of the I/U converter hardware delivered to the Heidelberg facility HIT.

The IBT electronics operates in two stages:

- Integration to accumulate the signal charge (10 pC full scale, given by 100 µs integration time and 100 nA full scale current)
- Conversion of the collected charge to a corresponding output voltage

Assuming a 0.1% ADC resolution (10 mV of 10 Volt full scale) leads to a charge resolution of 10 fC. This theoretical number is a factor of 25 smaller than that of the QFW (250 fC/count). A similar factor was estimated from measurements with Ni beam at HTP when the SEM grid was read out first with the QFW and then with the standard IBT electronics during the same beam time. The minimum particle number was ~$3x10^6$ particles for the I/U converter (range 12) and $1x10^8$ for the QFW.

1.4.2 QFW Electronics

The current QFW hardware has - by design - an intrinsic resolution of 250 fC/count. In principle, this resolution can be set to 25 fC/count, but this has not been tried yet. It is unlikely, that a full factor of 10 can be gained. This option will not be pursued!

To match very weak current signals to the QFW sensitivity the development of a pre-amplifier stage is planned. This external pre-amplifier unit would be inserted between detector and QFW input. The control of the gain setting can be implemented in the QFW hardware using existing features. The target is an improvement of the minimum particle numbers by a factor of 100 (effective sensitivity ~few fC/count).

Note:

- The Nickel data of section 2.1 yielded a roughly constant noise contribution of 100 counts in a 4 ms acquisition window in each of the 32 channels.
- This noise contribution was not constant over time, but appeared rather in small bursts during experiments. This effect was due to incorrect voltage settings in the DC/DC converter (see section 3.1) and was later reduced.
- Laboratory investigations on noise figures are presented in chapter 3, but do not change the order of magnitude of the minimum required particle number for practical applications. Noise depends on cable length, values of RC stretcher and total measurement time. For more information see table 6.

2 SEM Grid Measurements

2.1 Measurement with Nickel beam

2.1.1 Beam Parameters & Experiment Setup

The measurements were performed on 14th August 2014.

- Ion species: Ni, 26+
- Energy: 300 MeV/u
- Extraction: Fast, h=4
- Particle no.: 9E7 – 5E9 (6 runs of 50 cycles each)

- Resonant Transformer GHTPDT1 to monitor particle numbers via Python script (using CSCO Python module „devacc")

- Cromox Screen & SEM-Grid GHTPDG2 in same vacuum chamber
- SCR images recorded for comparison to SEM-Grid data

- FESA readout of 5 QFW units at HTP with modified GUI "LEBTProfile"
  - SFP2: 2 units for SEM-Grid GHTPDG2 with stretcher X+Y
  - SFP1: 2 units for GHTPDG3G (SEM-Grid in air) with stretcher X
  - SFP0: 1 unit for AirBPM (in AP container, ~75m RG214 cables)

- QFW settings:
  - Software delay 34 ms
  - Number of time slices 200
  - Total recording time 4 ms
  - Length of time slice 20 µs

2.1.2 Beam Profiles

Figure 2 shows repeated measurements of horizontal beam profiles for two beam intensities of 5E9 and 8E7 particles. The individual profiles are stacked in a 2D histogram. Profile data are presented according to wire number (wire ID) and not in coordinate space; the Cycle No. on the y-axis represents the measurement number.

Figure 3 (top) illustrates raw data for 8×10^7 particles. The data do not show a clear beam profile until integrated over the correct range of time slices. This yields the beam profile (bottom). From this plot one may set the detection threshold to about 1×10^8 particles for a meaningful measurement of beam position and width.

Figure 4 shows the raw data of Figure 3 (top) for channels 28 to 31. A regular pattern in the noise structure was apparent. Noise peaks were repeated every 50-60 time slices or roughly every ~1 ms. During laboratory investigations on noise the reasons were found and the noise contribution eliminated.

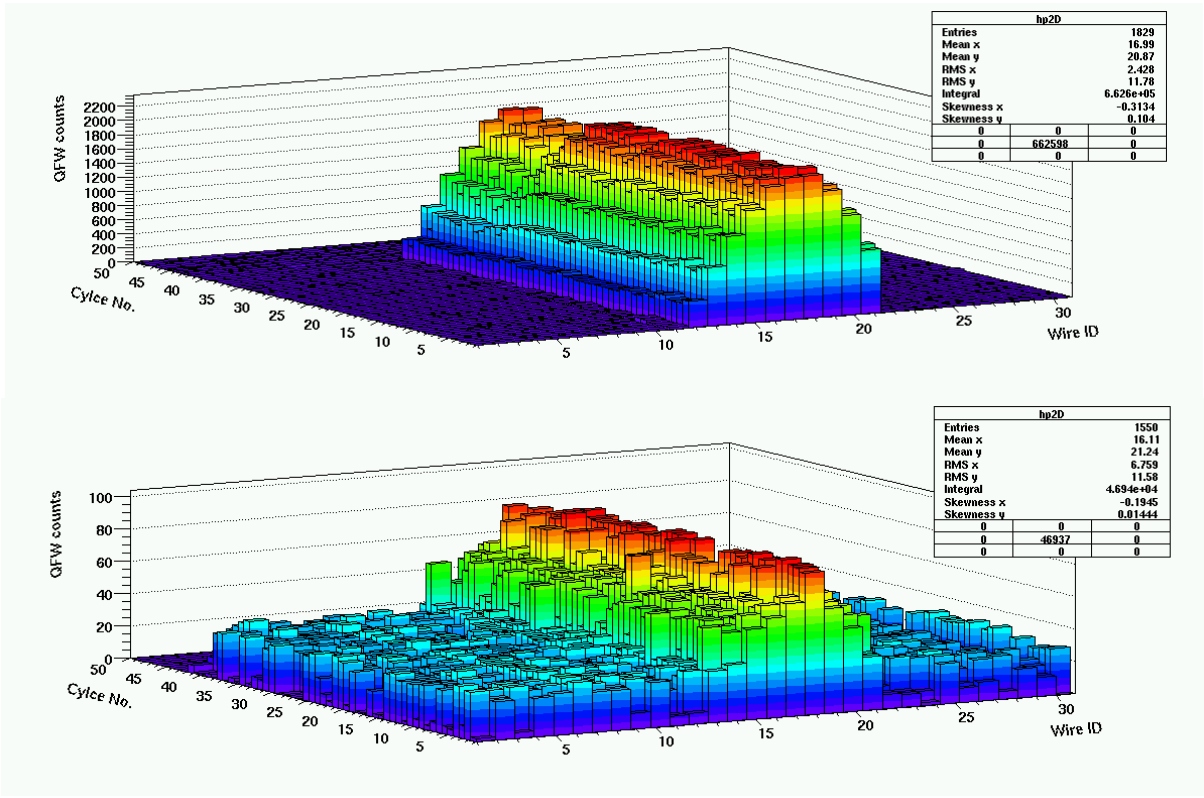

Figure 2: Sequence of profile measurements. Top: ~5E9 part./extraction; Bottom: ~8E7 part./extraction

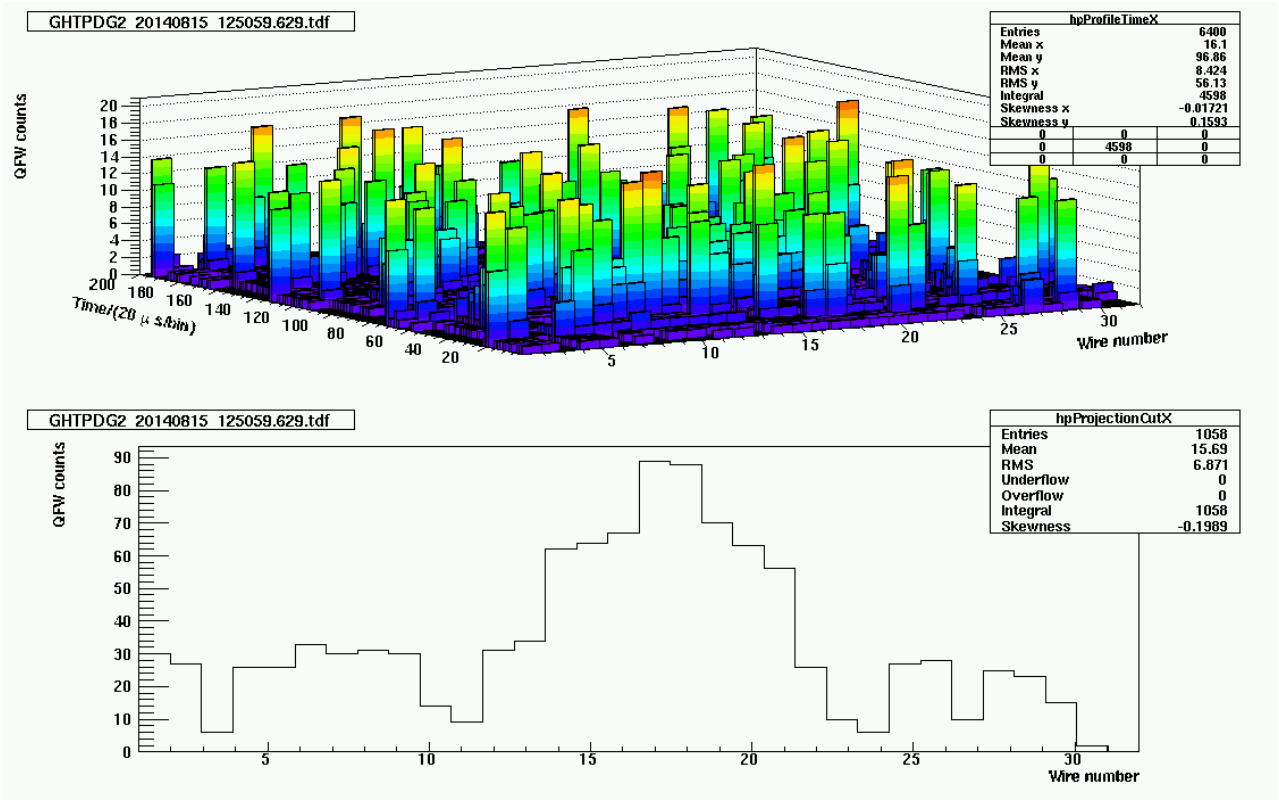

Figure 3: Raw data (top) for minimum intensity. The profile is hidden in the noise peaks. After selection of the correct time interval, the beam profile can be extracted (bottom).

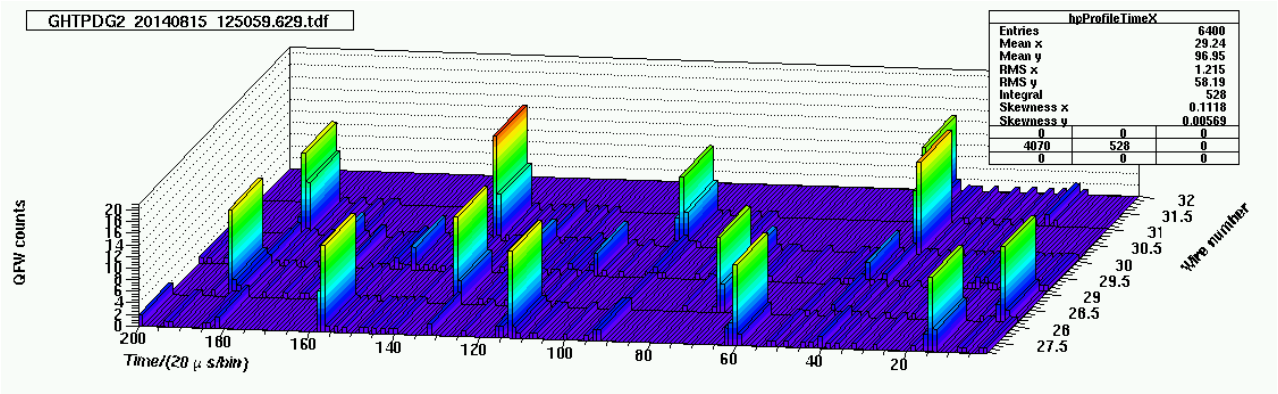

Figure 4: Enlarged area of the 2D raw data of Figure 3 showing the last 4 wire channels as function of time. Noise appears in somewhat regular intervals of 50-60 bins. This noise contribution was later eliminated (see section 3.1).

2.1.3 Charge Collection Time

Since the QFW measurement is based on the principle of counting, the hardware is unable to respond directly to the fast, intense current pulse generated by the beam. Therefore, the current must be fed to the QFW input via a pulse stretcher. Here we consider a simple RC circuit which has been inserted between the SEM-Grid cable and the QFW input.
The measured charge distribution is shown in Figure 5 for a beam of 5E9 particles, the highest possible particle number during measurement. Each of the 200 time slices is 20 µs long, the QFW sensitivity was set to 250 fC/count. The decay (or charge collection) time is roughly consistent with the estimated time constant of the RC circuit of ~100 µs. A total number of 14170 counts was registered which compares to the 17000 counts predicted by the analytical model.

From the data of Figure 5 one can estimate the maximum particle number at which saturation of the QFW output at 40 MHz occurs for a charge collection time of about 500 µs. The particle number of 5E9 must be multiplied by a factor 4000 (factor 1000 since QFW can be set to range 2500 fC/count, 1:10 current divider and factor 4 for full scale):

- Nickel, 300 MeV/u:2.0E13
- Uranium, 100 MeV/u: 1.0E12 (scaling of dE/dx, see Table 1 & Table 2)
- Protons, 2000MeV/u: 2.5E16 (scaling of dE/dx)

QFW rate R with initial QFW rate R_0 at time $t_0=0$
Decay constant $\tau \sim RC_{cap.}$ with R = 20 kOhm and $C_{cap.}$ the capacitance
Number of QFW counts $C_{QFW}(t)$

$$R(t) = R_0 \cdot \exp(-t/\tau)$$
$$C_{QFW}(t) = R_0 \cdot \tau \, [\, 1- \exp(-t/\tau) \,]$$

For an integration time $t(int) = 3\cdot\tau$, one obtains
$C_{QFW}(t=3\cdot\tau) \sim 0.95 \, (R_0\cdot\tau) \sim 95\%$ of the total charge

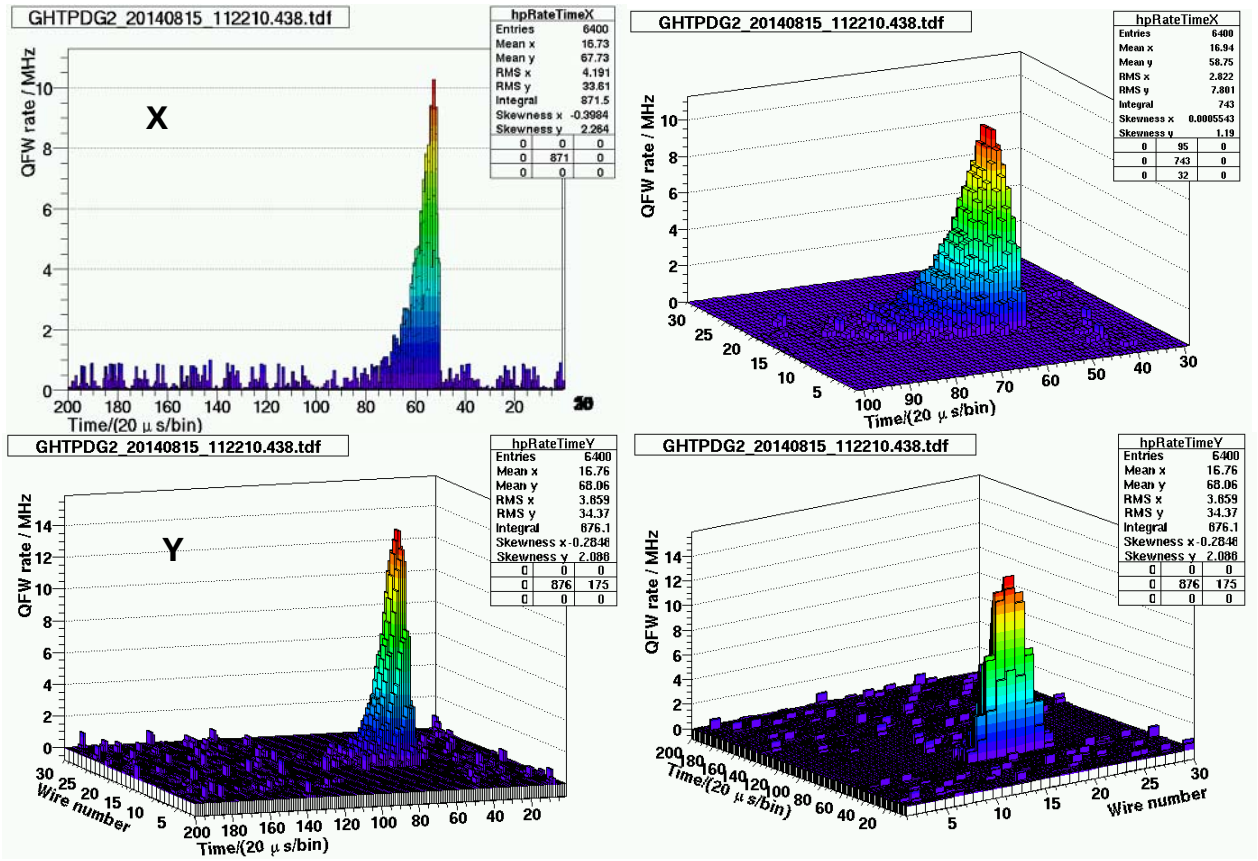

Figure 5: Time evolution of QFW input current with time axis orientation from right to left. Top: X plane; Bottom:Y plane. Each time slice is 20 µs long. The charge collection takes place within ~25 slices or 500 µs.

2.1.4 Comparison Simulation / Experiment

A Monte Carlo simulation has been written with a simple implementation of the DG090 SEM Grid geometry in the ROOT framework via the TGeometryManager class. User-defined vertex distributions can be selected, for example sampled from a Gaussian distribution or a 2D histograms of Cromox screen image. The particle momentum is perpendicular to the wire planes.

The ROOT Monte Carlo simulation is based on

- "geometric" particle tracking (straight line approximation),
- energy loss calculation by Atima code,
- Sternglass formula for primary SEM yield calculation,
- theoretical angular distribution of electron emission,
- ion charge at exit (equilibrium charge state according to Schiwietz),
- electron cross talk.

Events were sampled from 2D distribution measured by Cromox screen GHTPDF2 installed in front of GHTPDG2 (Figure 6). An offset adjustment of ~1mm was added to the Monte Carlo data in order to correct misalignment in the beam line.
The measured (blue, red) profiles are compared against the ROOT Monte Carlo simulation of the SEM emission for a DG090 grid in Figure 7. Simulation and experiment are normalised to 1E8 incident Ni particles of 300 MeV/u kinetic energy. Given the simplicity of the Monte Carlo model, the comparison between simulation and data is very satisfactory. Typically, the Monte Carlo results exceed the experimental yields by 30-80%.

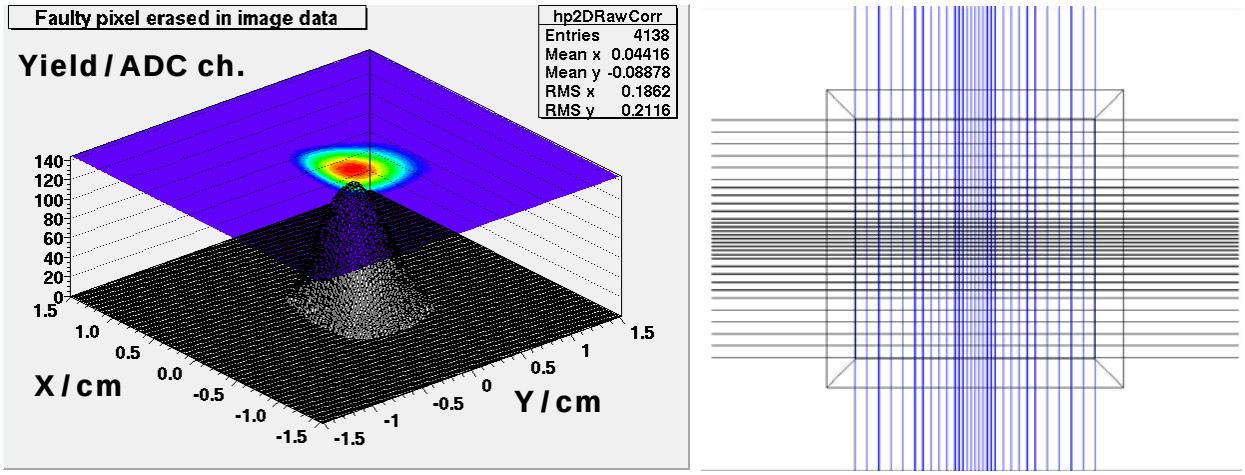

Figure 6: Cromox screen data after elimination of camera ADC offset (pedestal) outside the core distribution (left) and asymmetric wire geometry of DG090 profile grid (right).

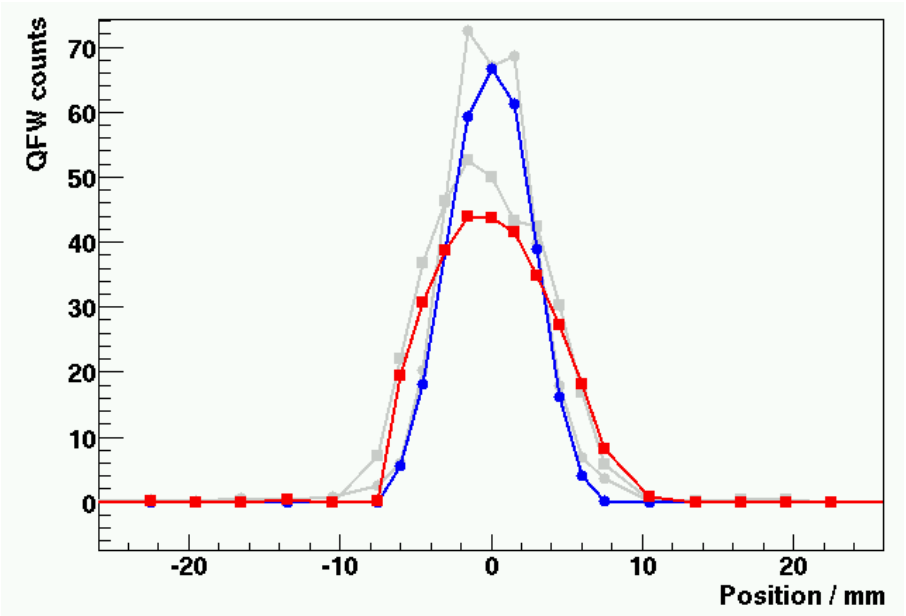

Figure 7: Comparison of measured and calculated SEM grid profiles, scaled to 10^8 incident particles. Gray: Monte Carlo calculation; Blue/Red: Data of horizontal/vertical profile.

2.1.5 Comparison SEM Grid & SCR Resolution

To illustrate the different spatial resolutions of SEM Grid and SCR detectors, Figure 8 presents two examples, one for a binning factor of 4 in the camera data and one for full camera resolution (~7 pixel/mm). The horizontal axis is given in units of mm. The dots represent the GHTPDG2 SEM Grid data, the back histogram the GHTPDF2 SCR data for a Nickel beam of ~3.5x10^7 particles of 300 MeV/u.

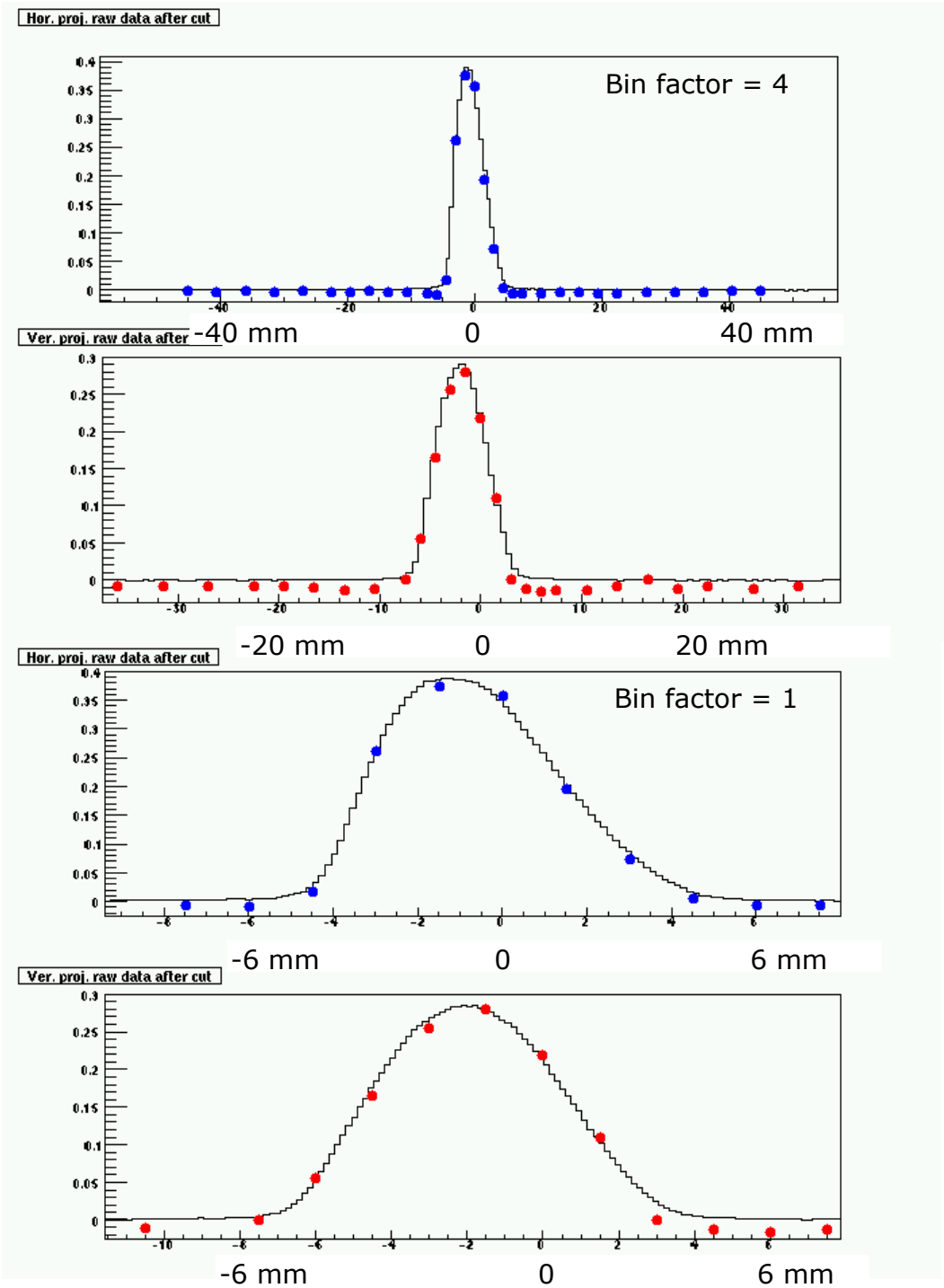

Figure 8: Comparison of beam profiles observed with Cromox screen GHTPDF2 (histogram) and SEM Grid GHTPDG2 & IBT Integrator electronics (dots).

2.2 Measurement with Xenon beam

2.2.1 Beam Parameters & Experiment Setup

- Ion species: Xe, 48+
- Energy: 300 MeV/u
- Extraction: Fast, h=4
- Particle no.: 7.7E7 – 1.4E9

- Resonant Transformer GHTPDT1 to monitor particle numbers
- HTPDG2 SEM-Grid
- 2 x POLAND-Units for 2x32 wires with RC-Stretcher
- Readout with MBS and GO4

2.2.2 Beam Profiles

Figure 9 and Figure 10 show measurements of horizontal and vertical beam profiles for two different particle numbers. The 2D-histrograms of X/Y profiles are presented according to wire number (wire ID), not in coordinate space. Using these figures one can set the QFW limit at ~8x10^6 Xe particles for the detection of a profile at a signal-to-noise ratio S/N~2.
In good agreement to the estimate of section 1.3.2, this value scales to 7.2x10^7 Ni ions to yield an equivalent S/N of ~3 as shown in Figure 3 (bottom) for 8x10^7 Ni.

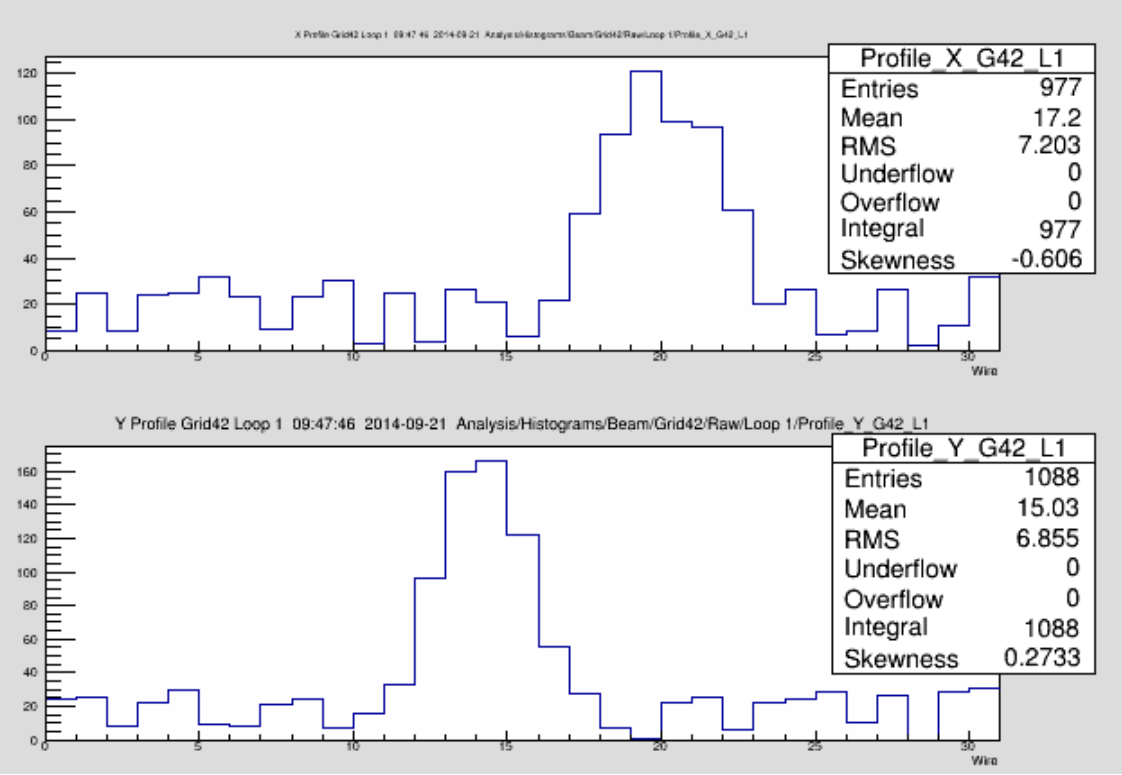

Figure 9: Horizontal and vertical profile with (S/N~5), ~ 3.6x10^7 particles, offset ~20 counts

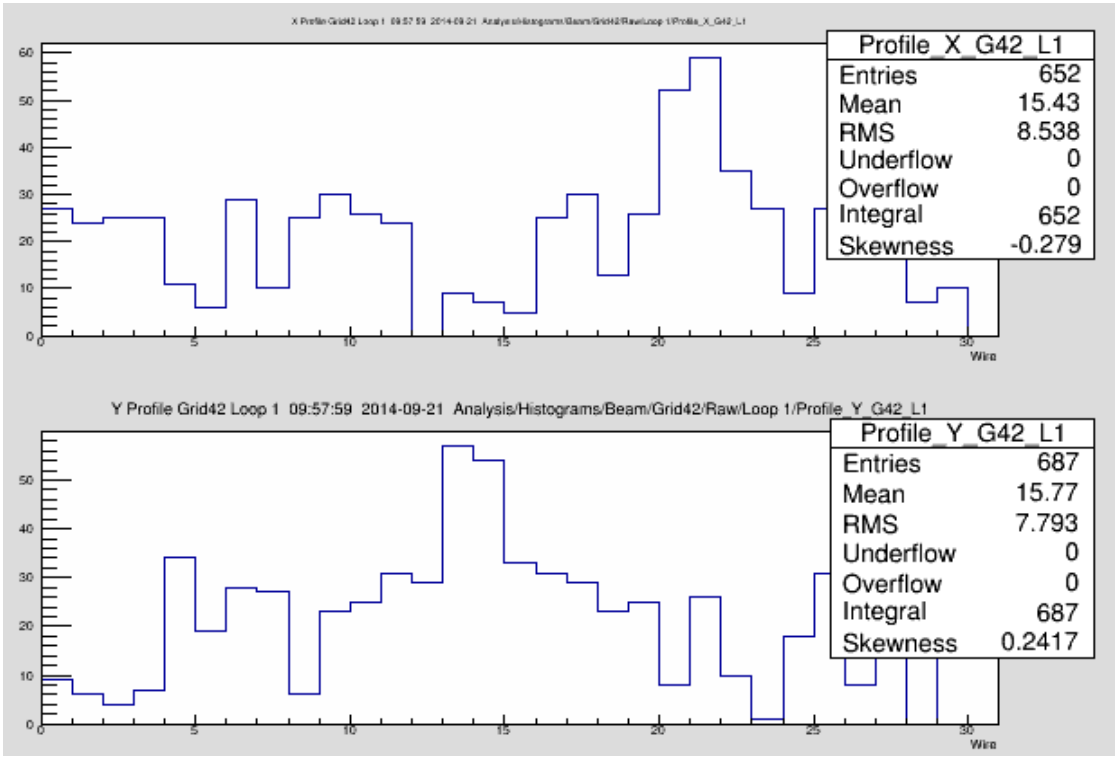

Figure 10: Horizontal and vertical profile (S/N ~2), ~7.7x10^6 particles; offset ~25 counts

3 QFW Noise Measurement

3.1 Noise reduction after lab investigation

Figure 11 shows an offset and noise measurement with a POLAND unit at HTP. The data of all QFW counts were added and in the diagram an oscillation of ~12 kHz frequency is apparent. Laboratory investigation proved that the dropout voltages of two DC/DC converters were too low. After dropout voltages had been increased, the oscillation was strongly reduced by a factor of ~6. The average QFW offset rate is about 225 kHz or 0.5% of the 40 MHz full scale value.

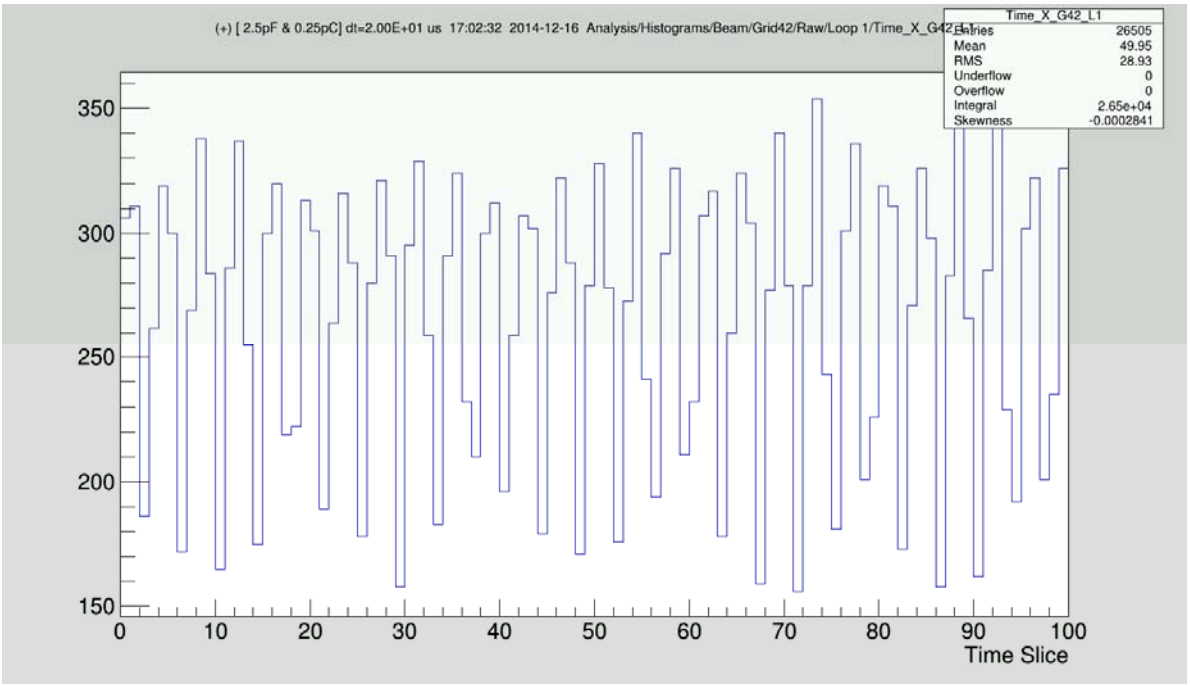

Figure 11: Measurement with POLAND unit without RC stretcher at 20 µs/ time slice. The plot shows the sum of all QFW counts as function of time for one cycle (DAC offset value 9000hex).

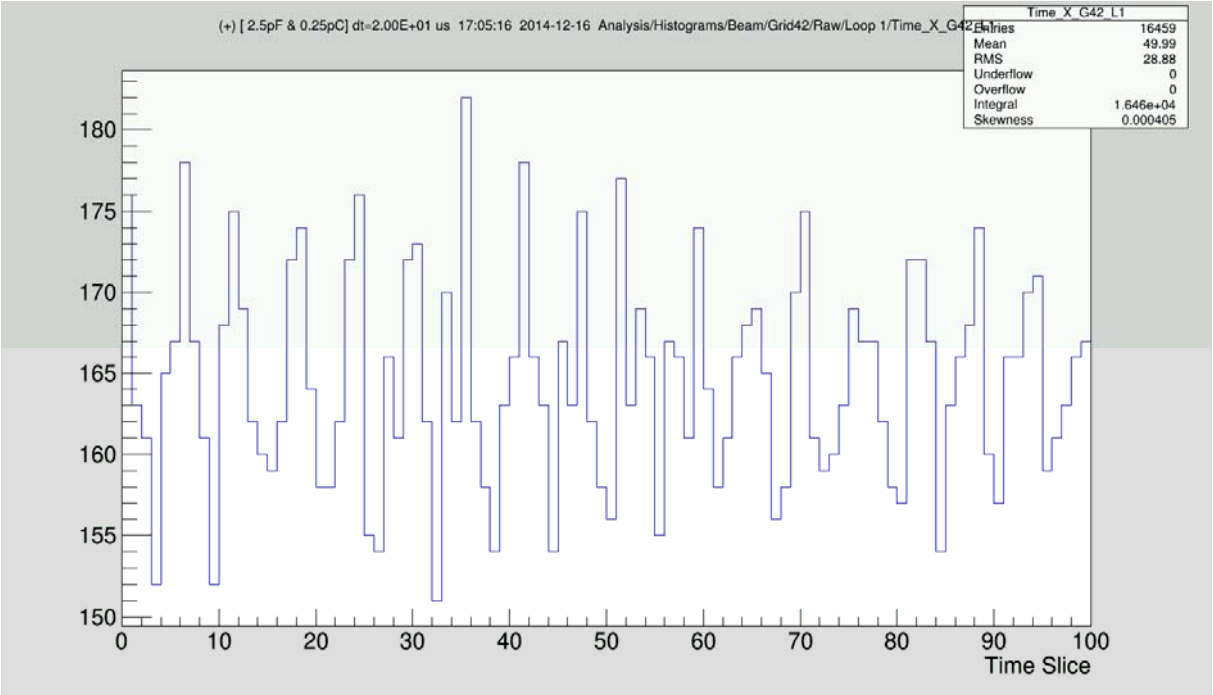

Figure 12: Same plot as before after increasing of dropout voltage from two DC/DC converters, for time slices of 20 µs length. The average QFW offset rate is ~225 kHz (5.6E-3 full scale).

3.2 Measurement Results

Table 4 presents noise data after dropout voltage correction for measurement intervals of 100 ms, 1 s and 10 s which represent typical values for slow extraction. 150 measurements were performed and the average standard deviation of a single QFW output calculated. Therefore, the stated values represent the uncertainty that has to be included to registered QFW counts when a background subtraction is performed.

The measurements were done without cable and detector. Here, the capacity values simulate the cable capacity of profile grid cables. The RC stretcher consists only of capacities and diodes. The diodes protect the QFW inputs and can be neglected in this case. The resistor of the RC stretcher arises from the input circuit of QFW (~20 kΩ). The tabulated values show that the noise is dependent on cable length and, hence, connecting cables should be kept as short as possible.

Table 4: This table presents noise values after noise reduction. Note that these values depend on cable length, measurement time and RC stretcher values. These measurements were taken without profile grid cable and SEM-Grid.

∑ Measurement time equates 100 Time Slices	Noise ± 1 σ / [QFW counts]	Equivalent charge [fC]
	RC stretcher with 0 nF (No PG cable)	
100ms	0.6	150
1s	1.1	275
10s	2.2	550
	RC stretcher with 4.7 nF (50 m PG cable)	
100ms	3.3	825
1s	4.3	1075
10s	4.9	1225
	RC stretcher with 470 nF (5000 m PG cable)	
100ms	8.8	2,2nF
1s	26.7	~6.6nF
10s	83.2	~20.8nF

4 Conclusions

- For fast extraction QFW hardware and passive RC pulse stretcher work as expected given the sensitivity of 250 fC/count. A roughly constant noise floor of about 20-30 counts was observed during Ni tests in a time interval of 30 time slices or 600 µs (section 2.1). This noise level later was reduced after optimisation of DC/DC supply voltages (section 3.1).
- The FESA readout worked reliably with 5 Poland units and 3 SFP ports (or 3 detectors).
- For the QFW, minimum particle numbers for different ions have been calculated from a simple model (Table 3) and verified experimentally with Ni and Xe beams of 300 MeV/u at HTP. The results agree when the data are normalised to the same S/N ratio and specific energy loss dE/dX.
- Maximum particle numbers for a charge collection time of ~600 µs have been estimated in section 2.1.3 on the basis of the measured profiles with Ni beam.
- For 10^8 protons, the required charge resolution is about 1 fC. However, it is questionable, if a SEM Grid is the correct choice of detector in this case.

Appendix I Comparison of yield estimate to published data

A selection of published electron emission yields has been compiled in Table 5. The last column states the backward yield Y_B as derived from Sternglass theory and ATIMA energy loss calculation. For comparison with total yields Y_T, these values can be multiplied by 2, assuming identical forward and backward yields. There is a general lack of measurements in the 10-100 MeV/u range. Some data were taken from GSI publications of the FRS collaboration and measurements with a CERN BLMS at HTP.

Table 5: Published SEE yield of various authors. The last column gives the backward yield calculated from Sternglass model and energy loss by ATIMA.

Ref	Ion / Energy / (MeV/u)	Target / Thickn. / (µg/cm^2)	Yields Y_F / Y_B for- / backward	Yield Y_B Sternglass+Atima
[3]	U^{68+}/ 8	C foil / 44	400	390
[2]	U^{68+} / 8	C foil / 44	2000±800 / 470±200	390
	U^{38+} / 3.5	C foil / 44	1300±500 / 630±250	407
	Ne^{10+} / 3.5	C foil / 20	26 / 10	24
	Ne^{7+} / 8.5	C foil / 100	16±3 / 6.2±1.5	13.5
[4]	H^+ / 1.2	Carbon	1.2 / 1	0.7
	H_2^+ / 1.2	Carbon	2.8 / 3.2	1.4
[6]	Au^{24+} / 11.4	Carbon	330 / ----	299
[8]	O^{5+} / 1.5	Carbon / 20	$Y_T = Y_F + Y_B = 46$	26
	O^{5+} / 1.0	Carbon / 20	$Y_T = 55$	31
	O^{4+} / 0.5	Carbon / 20	$Y_T = 62$	37
	$C^{3+/4+}$ / 1.85	Carbon / 20	$Y_T = 28$	15
	$C^{3+/4+}$ / 1.0	Carbon / 20	$Y_T = 37$	20
	$C^{3+/4+}$ / 0.5	Carbon / 20	$Y_T = 46$	26
	$Li^{2+/3+}$ / 2	Carbon / 20	$Y_T = 12$	4.2
	$Li^{2+/3+}$ / 1.15	Carbon / 20	$Y_T = 15$	5.9
	$Li^{2+/3+}$ / 0.5	Carbon / 20	$Y_T = 22$	9.3
	p / 0.8, 1.6	C, thin Al Ni Au	Y_T given in Fig. 1 and Fig. 2 of ref. [8] Good agreement with calculation	0.9 / 0.6 1.2 / 0.6 1.5 / 0.9 1.7 / 1.2
[9]	p / 1.0-7.0	Carbon	Y_F / Y_B Fig. 2	Good agreement with Y_B data
[13] [14]	P / 450000	Ti	Y_T = (3.60±0.07)% Y_T = (3.5-4.1)%	Y_B = 1.7 %
[15]	Xe / 600	Al	Y_T = 116±2.3	Y_B = 32.2
[16]	C / 195	Ti	Y_T = 3.8	Y_B = 0.9
[17]	Ar / 300	Ti	Y_T = 8.8±0.4	Y_B = 8.1
	C / 300	Ti	Y_T = 0.9±0.1	Y_B = 0.75
	U / 500	Ti	Y_T = 321±3	Y_B = 138
	U / 320	Ti	Y_T = 354±15	Y_B = 168
[19]	Cu / 9.6	C foil / 1000	Y_B = 60 / Y_F = 170	Y_B = 79
	Ni / 74	C foil / 1000	Y_B = 22 / Y_F = 60	Y_B = 19

Appendix II Comparison of charge estimate to SEM grid data

Data recorded with different SEM grid geometries and with different ions and energies are compared in Table 6. The GSI UNILAC data was measured with the new QFW hardware, all other data with the IBT current-to-voltage converter, a charge integrator, which currently is the standard electronics at GSI.

Table 6: Charge comparison between model and data

GSI UNILAC (2011-2013)						
Ion	***Q***	***Energy (MeV/u)***	***Trafo (µA) UX2DTA***	***Counts X/Y Plane***	***Counts Model***	***QFW (pC/pulse) Sensitivity***
124-Xe	+21	4.773	980 (3.1×10^{10})	7080/7100	7830 (+10%)	25 (1/10 current div.) 1.5 mm wire sep.
			5.9 (1.9×10^{8})	281/263	472 (+70%)	2.5
			2.0 (6.3×10^{7})	85/105	160 (+88%)	2.5
238-U	+39	8.624	~65 (1.1×10^{9})	3570/3280	5160 (+45%)	2.5 (~2070 e-/ion)
	+28	11.4	~20	2093	2210	2.5
GSI High Energy Beam Line HTP (2014)						
58-Ni	+26	300.0	$3.5\text{x}10^{7}$	27 pC	32 pC (+18%)	IBT Integrator Range 11
HIT Therapy Facility Heidelberg (2012)						
Ion	***Q***	***Energy (MeV/u)***	**Faraday Cup**	**Charge X/Y plane**	**Model Charge**	**Comment**
Proton	+1	7.0	525 nA	5.5/5.3 pC	6.7 pC (+24%)	100 µs integration 1.1 e-/proton 78/100 µm = mean/total wire thickness 1.2 mm wire sep.
CNAO Therapy Facility Pavia (2007-2009)						
Ion	***Q***	***Energy (MeV/u)***	**Trafo**	**Charge X/Y plane**	**Current Model**	
12-C	4+	0.4	61.3 µA	3.6/4.0 pC	5.1 pC (+34%)	37.1 e-/ion 1.2 mm wire sep.
12-C	4+	7.0	78.8 µA	4 pC	3.3 pC (-20%)	
3-H	1+	0.4	500 µA	~37 pC	40 pC (+8%)	Assume molecular break-up (x3)
3-H	1+	7.1	300 µA	8-9 pC	7.2 pC (-15%)	break-up (x3)

References

[1] H. Rothard et al., Phys. Rev. A, Vol. 41, No. 5, 2521ff., 1990
[2] D. Schneider et al., Phys. Rev. A, Vol. 47, No. 5, 3945ff., 1992
[3] R.A. Sparrow et al., J. Phys. B: At. Mol. Opt. Phys. 28 (1995) 3427-3429
[4] Kroneberger et al., NIM B29 (1988) 621-626
[5] Hippler et al., NIM B34 (1988), 518-520
[6] Rothard et al., NIM B258 (2007), 91-95
[7] Hasselkamp et al., NIM 180 (1981), 349-356
[8] A. Clouvas et al., Phys. Rev. B, Vol. 39, No. 10, 6316ff., 1989
[9] A. Clouvas et al, Phys. Rev. B, Vol. 55, No. 18, 86ff., 1997
[10] ATIMA, http://web-docs.gsi.de/~weick/atima/
[11] G. Schiwietz, P.L. Grande, NIM B 175-177 (2001) 125-131
[12] G. Schiwietz et al., NIM B 226 (2004) 683-704
[13] K. Bernier et al., CERN Report 97-07, July 1997
[14] G. Ferioli, R. Jung, CERN Report CERN-SL-97-71(BI), December 1997
[15] A. Junghans et al., NIM A370 (1996) 312-314
[16] B. Jurado et al., NIM A483 (2002) 603-610
[17] A. Reiter, GSI Internal Report, July 2011
[18] E.J. Sternglass, The Physical Review, Vol. 108, No. 1, 1957
[19] M. Jung, et al., Phys. Rev. A, Vol. 54 (No. 5), November 1996